Available online at www.sciencedirect.com

ScienceDirect

journal homepage: www.elsevier.com/locate/he

Enhanced electrochemical activity of Co_3O_4/Co_9S_8 heterostructure catalyst for water splitting

Nadeem Asghar Khan [a,1], Iqbal Ahmad [a,b,**,1], Naghmana Rashid [a], Muhammad Nadeem Zafar [c,*], Farooq Khurum Shehzad [d], Zahid ullah [e], Anwar Ul-Hamid [f], Muhammad Faizan Nazar [g], Muhammad Junaid [h], Muhammad Faheem [i], Syed Salman Shafqat [j], Uzma Jabeen [k], Alaa Dahshan [l,m]

[a] Department of Chemistry, Allama Iqbal Open University, Islamabad 44000, Pakistan
[b] School of Chemical Engineering and Technology, Xi'an Jiaotong University, Xi'an 710049, China
[c] Department of Chemistry, University of Gujrat, Gujrat 50700, Pakistan
[d] Department of Chemistry, Muhammad Nawaz Sharif University of Engineering and Technology (MNSUET), Multan 60000, Pakistan
[e] Department of Environmental Science, Allama Iqbal Open University, Islamabad 44000, Pakistan
[f] Core Research Facilities, Research Institute, King Fahd University of Petroleum & Minerals, Dhahran 31261, Saudi Arabia
[g] Department of Chemistry, Division of Science & Technology, University of Education, Lahore, Multan Campus, Pakistan
[h] College of Physics, Changchun University of Sciences and Technology, Changchun 130000, China
[i] School of Chemistry, Northeast Normal University, Changchun 130000, China
[j] Department of Chemistry, Division of Science & Technology, University of Education, Lahore 54770, Pakistan
[k] Faculty of Basic Sciences, Sardar Bahadur Khan Women's University Quetta 87300, Pakistan
[l] Department of Physics, Faculty of Science, King Khalid University, P.O. Box 9004, Abha, Saudi Arabia
[m] Department of Physics, Faculty of Science, Port Said University, Port Said, Egypt

HIGHLIGHTS

- A novel Co_3O_4/Co_9S_8 catalyst exhibited the excellent performance for water oxidation.
- The Co_3O_4/Co_9S_8 catalyst exhibits a favorable OER with 281 mV of overpotential.
- A small Tafel slope of 37 mV dec^{-1} achieved for Co_3O_4/Co_9S_8 electrocatalyst in alkaline media.
- The Co_3O_4/Co_9S_8 catalyst has low Tafel slope and overpotential than most state of art Co-based electrocatalysts.

GRAPHICAL ABSTRACT

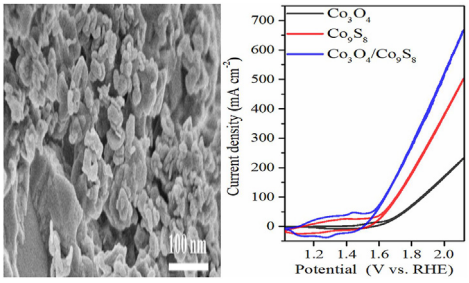

* Corresponding author.
** Corresponding author. Department of Chemistry, Allama Iqbal Open University, Islamabad 44000, Pakistan.
E-mail addresses: iqbal.ahmad@aiou.edu.pk, iqbalahmadchem@gmail.com (I. Ahmad), nadeem.zafar@uog.edu.pk, znadeempk@gmail.com (M.N. Zafar).
[1] Authors have equal contributions.

https://doi.org/10.1016/j.ijhydene.2021.11.124

ARTICLE INFO

Article history:
Received 24 June 2021
Received in revised form
1 November 2021
Accepted 15 November 2021
Available online 8 December 2021

Keywords:
Cobalt sulfide
Cobalt oxide
Heterostructures
Water oxidation
Oxygen evolution reaction

ABSTRACT

The dearth of efficient, robust, and economical electrocatalysts for water oxidation is dubiously the key obstacle for renewable energy devices, so synthesis of efficient, and cost-effective metal-based water oxidation catalysts is vital. Herein, Co_3O_4, Co_9S_8 catalysts and their heterostructure Co_3O_4/Co_9S_8 were synthesized and evaluated as water oxidation electrocatalysts. The characterization of Co_3O_4, Co_9S_8, and Co_3O_4/Co_9S_8 electrocatalysts was performed using Fourier transform infrared spectroscopy, scanning electron microscopy and X-ray diffraction techniques. The heterostructure Co_3O_4/Co_9S_8 (1.46 V) exhibited water oxidation electrocatalysis at extremely low onset potential compared to Co_3O_4 (1.58 V), and Co_9S_8 (1.48 V) catalysts. A 281 mV overpotential required to attain a current density of 50 mA cm^{-2} in alkaline solution (1 M KOH), outperforming most of Co-based benchmark electrocatalysts. Further, the Co_3O_4/Co_9S_8 heterojunction demonstrated catalytic activity with small Tafel slope of 37 mV dec^{-1}. The finding of electrochemical studies involving controlled potential electrolysis and long-term stability are projected to steer the future advancement in constructing efficient, economical, stable, and earth-abundant metal-based water oxidation catalysts.

Introduction

Sustainable solutions to the impending energy crisis are attaining great attention of the researchers because of rapidly diminishing reserves of fossil fuels and their adverse effects on ecosystem [1–4]. Thus, it is vital to discover green and renewable energy resources to meet the ever-growing energy demands of the world [5,6]. Hydrogen production is the most convenient way to store clean energy if it is not obtained by reforming of methane which accompanying carbon dioxide pollution. Electrochemical water splitting generates hydrogen at cathode and oxygen at anode of the electrolyzer which is current focus of the research in this field [7,8]. The catalysts for hydrogen evolution reaction (HER) and oxygen evolution reaction (OER) facilitate the production of hydrogen and oxygen through electrochemical water oxidation, which is thought to be sluggish kinetically [9]. So effective water oxidation electrocatalysts are needed to boost water splitting process, to reduce the overpotential and to augment the conversion efficiency. In designing of active electrocatalysts, two barriers i.e. the poor stability of the OER catalysts and the high overpotentials has to overcome for large scale efficient water oxidation [10].

Electronic and structural modification has done previously in literature to tune the efficiency of electrocatalysts for better OER [11–15]. Currently, compounds of Pt and noble metal oxides such as RuO_2, IrO_2 are best electrocatalysts for oxygen reduction reaction (ORR) and OER, respectively [16,17]. The paucity and high price of noble metals and their compounds limits their broad applications. Thus, it is highly desirable to develop earth abundant, highly active, stable, and inexpensive electrocatalysts [10,18–20]. Recently carbon based electrocatalysts have been reported as an alternative to metal-based catalysts, which showed improved OER and HER performance [21–24]. Further considering the highly active, stable, and inexpensive compounds, the transition metals afford new substitutes to produce new OER electrocatalysts [25–30]. Among transition metals, cobalt offers the foundation for the development of suitable electrocatalyst especially because of 3d electronic properties, the oxides, and the sulfides of cobalt such as CoS_2, Co_3S_4 and Co_3O_4 have gained most attractive attentions [31–33]. However, to drive the OER process, high overpotential is the major obstacle which limits charge transfer due to inherent poor conductivity in oxides of cobalt [34,35]. Although cobalt sulfides ensure faster charge transfer, but poor stability in basic media still prevents their application [36–38]. Based on the above analyses, it is anticipated that the synergism of highly conductive, active sites enriched, and highly stable cobalt-based compounds could be good candidate for novel catalysts.

Considering the above-mentioned concerns, fabrication, and production of novel heterostructures is very crucial to search for electrocatalysts with enhanced electrocatalytic performance for water splitting. Furthermore, Co-based sulfides and oxides are the earth abundant electrochemical water oxidation electrocatalysts under alkaline conditions and have been proven as economical catalysts. In this study Co_3O_4/Co_9S_8 heterostructure and its counterparts Co_3O_4/Co_9S_8 were synthesized and characterized using different techniques for instance scanning electron microscopy (SEM), Fourier transform infrared spectroscopy (FTIR), and X-ray diffraction (XRD). Chronoamperometry and Cyclic voltammetry (CV) techniques were utilized to study the electrochemical properties and catalytic activity of synthesized electrocatalysts. A through literature survey indicates that no reports on Co_3O_4/Co_9S_8 heterostructure as electrocatalyst for water splitting are found but only few studies, where Co_9S_8 has been assembled onto Co_3O_4 to make hybrid electrocatalyst for OER [39,40]. Further the finding of electrochemical studies revealed that the water oxidation ability of Co_3O_4/Co_9S_8 heterostructure is outperforming most of the Co-based electrocatalysts reported so far.

Experimental

Materials

Sodium sulphide penta-hydrate ($Na_2S.5H_2O$, 98%) and sodium hydroxide (NaOH) were obtained from Daejung Chemicals (Siheung-si, South Korea). Potassium hydroxide (KOH, 99%) was purchased from Scharlab (Barcelona, Spain) and cobalt nitrate hexa-hydrate ($Co(NO)_3.6H_2O$, >99%) was obtained from BDH Chemical Ltd. Nickel foam (thickness = 0.5 mm, porosity = 98%) was obtained from Shenzhen Lifeixin Environment Material Co. Ltd. whereas Nafion solution (5 wt%) was purchased from Sigma–Aldrich.

Synthesis of Co_3O_4, Co_9S_8 and Co_3O_4/Co_9S_8 catalysts

Hydrothermal method was employed to synthesize all the catalysts. For the synthesis of Co_3O_4 nanorods, 0.5 M solution of $Co(NO)_3.6H_2O$ was prepared in 20 mL distilled water and uninterruptedly agitated for about 30 min. In next step, the solution pH was maintained at 12 through dropwise addition of 2 M NaOH solution. Then the resultant mixture was put into a 50 mL stainless steel Teflon lined autoclave filled up to 70% of volume and heated at 180 °C in an oven for 16 h. The prepared catalyst was filtered, washed with deionized water several times, and dried overnight in an oven at 80 °C. the obtained product was calcinated for 1 h at 500 °C to get the Co_3O_4 nanorods.

To synthesize Co_9S_8 catalyst, 12 mL of 0.5 M Na_2S solution was mixed with 12 mL of 0.5 M $Co(NO)_3.6H_2O$ solution in a beaker followed by successively agitation for 1 h at room temperature. After that the resultant mixture was subjected to heat in an oven at 180 °C for 16 h using stainless steel Teflon lined autoclave. The prepared catalyst was filtered and dried in an oven at 60 °C for 12 h.

For the synthesis of heterostructure Co_3O_4/Co_9S_8, the Co_3O_4 nanorods were dispersed in 10 mL of 0.5 M of $Co(NO_3.)6H_2O$ solution followed by sonication for 30 min in order to get homogeneous suspension. Then, the suspension was stirred at ambient temperature for 1 h while dropwise addition of 10 mL of 0.5 M Na_2S solution. The required catalyst was obtained by performing reaction at 180 °C for 16 h in an oven using stainless steel Teflon lined autoclave. Lastly, the heterostructure was collected by filtration and dried at 80 °C in an oven.

Characterization of Co_3O_4, Co_9S_8, and Co_3O_4/Co_9S_8 catalysts

To track out the crystal structure and size, XRD analysis was performed on a Rigaku SmartLab X-ray diffractometer (Rigaku Beijing Corporation, Beijing, China) using Cu-Kα radiation functioning at a 30 mA current and 40 kV voltage. The morphological information of catalysts was obtained by performing SEM analysis using a Hitachi SU8010 microscope (Hitachi High-Technologies Corporation, Tokyo, Japan). FTIR measurements were performed using a Nicolet 1S50 110 V/InGaAs spectrometer (ThermoFisher Scientific, Waltham, USA).

Electrochemical measurements of Co_3O_4, Co_9S_8, and Co_3O_4/Co_9S_8 catalysts

An electrochemical workstation (Autolab PGSTAT 302, Utrecht, The Netherland) was used to execute all the electrochemical experiments in a conventional 3-electrode electrochemical cell. The Ni-foam (2×2 cm^2) modified with the samples (Co_3O_4, Co_9O_8 and Co_3O_4/Co_9O_8 electrocatalysts), Ag/AgCl and Pt wire were applied as working electrode, reference electrode, and counter electrode, respectively. For all the electrochemical measurements, 1 M KOH solution as electrolyte was used. For linear sweep voltammetry (LSW) and CV measurements were made by applying a scan rate of 5 mV s^{-1}. Eq. (1) was used to perform the calibration of all the potentials.

$$E_{RHE} = E_{Ag/AgCl} + (0.1976 + 0.059\ pH)V \quad (1)$$

The overpotential values of Co_3O_4, Co_9O_8 and Co_3O_4/Co_9O_8 electrocatalysts for water oxidation were estimated by sing Eq. (2).

$$\eta = E_{RHE} - 1.23\ V \quad (2)$$

where η represents the overpotential. The Eq. (3) was applied to calculate the Tafel slopes.

$$\eta = b\ Log\ j + a \quad (3)$$

where a, b and j represent the constant, Tafel slope and current density, respectively.

Controlled potential electrolysis was also performed under stationary conditions using chronoamperometry. Electrochemical impedance spectroscopy (EIS) was executed using 100 kHz–10 mHz frequency range at open circuit potential by setting amplitude value at 5 mV [41,42]. Solution resistance and charge transfer resistance values have been calculated by fitting the impedance data using following simplified Randles model (Fig. 1). For the fabrication of working electrode (Ni-foam), 5 mg mL^{-1} solution/suspension of electrocatalyst was prepared in ethanol by applying sonication for 1 h. Next that 5 wt% solution of Nafion was prepared and 10 μL was mixed in resultant electrocatalyst dispersion. Next, on both sides of working electrode (Ni-foam with dimension 2×2 cm^2), this synthesized electrocatalyst was drop-casted and stored at room temperature overnight.

Results and discussion

Characterization of Co_3O_4, Co_9S_8, and Co_3O_4/Co_9S_8 catalysts

To confirm structures of nano-electrocatalysts, powder XRD studies have been performed [43–45]. Fig. 2 shows XRD

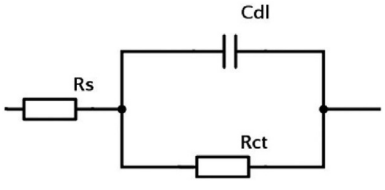

Fig. 1 – Simplified Randles circuit.

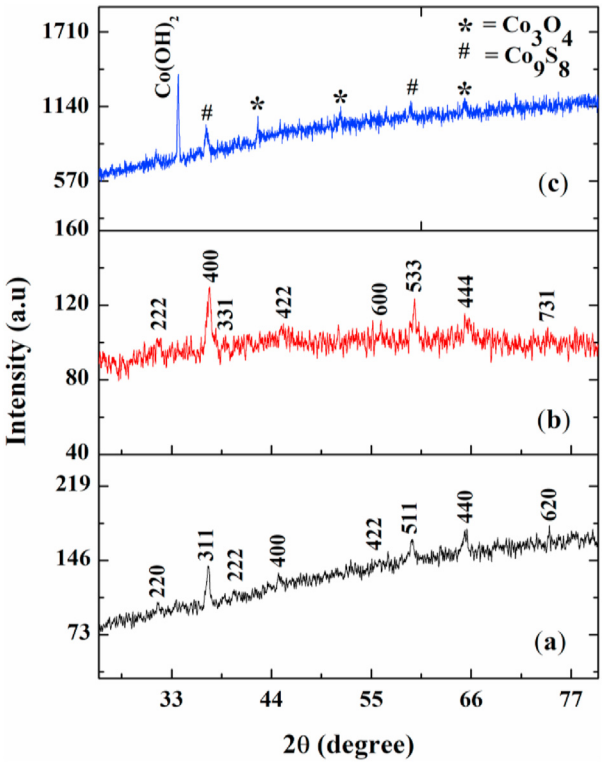

Fig. 2 – X-ray diffractograms of (a) Co_3O_4, (b) Co_9S_8, and (c) Co_3O_4/Co_9S_8 electrocatalysts.

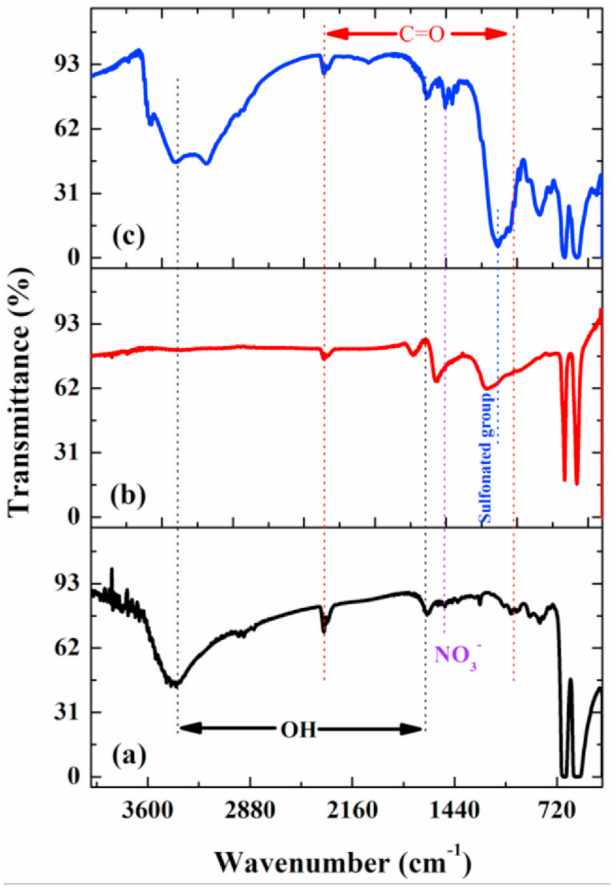

Fig. 3 – FTIR spectra of (a) Co_3O_4, (b) Co_9S_8, and (c) Co_3O_4/Co_9S_8 electrocatalysts.

spectra of cobalt oxide, cobalt sulfide, and cobalt oxide/cobalt sulfide nanocrystals. XRD spectrum of cobalt oxide (Fig. 2a) reveals diffraction peaks at 2θ values of 31.4°, 36.9°, 39.8°, 44.7°, 55.9°, 59.3°, 65.6°, and 74.4° and correspond to planes (220), (311), (222), (400), (422), (511), (440), and (620), respectively (JCPDS card No. 009-0418). This diffraction pattern indicates the formation of typical cubic spinel phase of Co_3O_4 [46,47]. Diffraction peaks of cobalt sulfide (Fig. 2b) at 2θ values of 31.5°, 36.94°, 39.42°, 45.32°, 55.83°, 60.15°, 65.24°, and 73.85° shows a fair degree of crystallinity and these peaks are indexed to (220), (400), (331), (422), (600), (533), (444), and (731) planes of cubic phase of Co_9S_8 (JCPDS card No. 002-1459) [46]. In XRD spectrum of Co_3O_4/Co_9S_8 (Fig. 2c), diffraction peaks of both Co_3O_4 as well as Co_9S_8 are present and indicate the formation of Co_3O_4/Co_9S_8 heterostructure. An intense peak at 33.2° is attributed to β-$Co(OH)_2$ [48]. In a previous report, Tong et al. vulcanized Co_3O_4 sample with Co_9S_8 to produce hybrid Co_3O_4@Co_9S_8 electrocatalyst for water splitting. The Co_3O_4 sample was spinal shaped as per JCPDS card No. 42-1467 in Co heterostructure [39]. The Co_3O_4/Co_9S_8 heterostructure reported in this study is also comparable except the Co_3O_4 sample was cubic phase as per JCPDS card No. 009-0418.

FTIR is useful technique for identification of different types of surface functional groups from 4000 to 400 cm^{-1} wavenumber [49]. In Fig. 3, FTIR spectra of Co_3O_4, Co_9S_8, and Co_3O_4/Co_9S_8 catalysts are shown. FTIR spectra of all catalysts show the presence of two absorption bands i.e. at 3399 cm^{-1} attributing to stretching and 1636 cm^{-1} to bending vibrations of adsorbed water on surface of samples [50,51]. Similarly, the peaks observed at 2350 and 1040 cm^{-1} are due to the adsorbed carbon dioxide from the atmosphere [52]. For Co_9S_8 and Co_3O_4/Co_9S_8, the peak observed at 1144 cm^{-1} is credited to bending vibration of sulfonated group of Co_9S_8 [53] and is merged with CO_2 absorption band. In all FTIR spectra, the peak appearance at about 1450 cm^{-2} correspond to NO_3^-, which possibly is adsorbed in samples and perhaps is not removed completely by washing [54]. For Co_3O_4 (Fig. 3a), two particular absorption bands observed at 676 and 574 cm^{-1} are due to stretching vibrations for Co (II)-O and Co(III)-O, respectively, in spinel structure of Co_3O_4 [55]. For Co_9S_8 and Co_3O_4/Co_9S_8, peak found at 838 cm^{-2} is ascribed to stretching vibration of Co-S bond [56]. It is worth mentioning that the peaks of Co-O bonds are also present in FTIR spectrum of Co_9S_8 due to presence of $Co(OH)_2$, which is in accordance to the XRD results.

Surface morphological features and microstructure of the prepared catalysts have been studied by SEM. Fig. 4 indicates the SEM micrographs of Co_3O_4, Co_9S_8, and Co_3O_4/Co_9S_8 catalysts. It is clear from the SEM image in Fig. 4a that Co_3O_4 possesses hexagonal rods with different sizes, distributed randomly and the average size of Co_3O_4 rods is approximately 80 nm Co_9S_8 particles (Fig. 4b) are looks like cabbage nanosheets. The nanosheet combined to produce porous material of large surface area, which accelerates the OER. In the SEM micrograph of Co_3O_4/Co_9S_8 heterostructure (Fig. 4c), hexagonal rods of Co_3O_4 are embedded in the nanosheets of

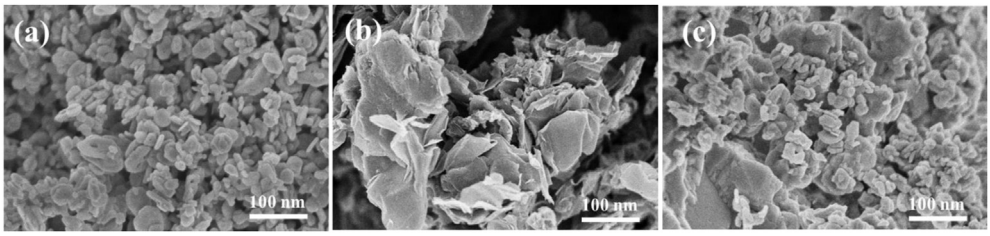

Fig. 4 – SEM micrographs of (a) Co_3O_4, (b) Co_9S_8, and (c) Co_3O_4/Co_9S_8 electrocatalysts.

Co_9S_8. The cavities present in Co_3O_4/Co_9S_8 heterostructure serve as reservoirs for electrolyte which boosts the OER.

Electrochemical studies of Co_3O_4, Co_9S_8, and Co_3O_4/Co_9S_8 catalysts

After detail characterization of nanomaterials, water electrocatalytic oxidation performance of Co_3O_4, Co_9S_8, and Co_3O_4/Co_9S_8 catalysts has been measured. To execute this, the catalysts are tailored on Ni-foam and the electrochemical studies are measured in 1.0 M KOH by running LSV and CV at 5 mV s^{-1} scan rate. The *iR* uncompensated linear sweep voltammograms (LSVs) and cyclic voltammograms (CVs) of working electrode (Ni-foam) fabricated with Co_3O_4, Co_9S_8, and Co_3O_4/Co_9S_8 electrocatalysts are shown in Fig. 5. The Fig. 5A reveals that during anodic potential sweep of CV, a small oxidation peak of Co_3O_4 centered at E_{pa} of 1.53 V (vs. RHE) is identified suggesting the peroxidation feature of water. The LSV of Co_3O_4 also displays similar behavior of Co_3O_4 oxidation and showing anodic peak at around E_{pa} = 1.53 V (vs. RHE). A very small reduction peak of Co_3O_4 is seen during the reverse scan of CV, which reveals that the reaction is somewhat reversible. The CV of Co_9S_8 shown in Fig. 5A exhibits a reduction peak at E_{pa} of 1.24 V (vs. RHE) during cathodic potential sweep of CV and an oxidation peak is detected at E_{pa} of 1.41 (vs. RHE) during forward potential sweep of CV. A similar oxidation peak of Co_9S_8 is also observed during its LSV scan (Fig. 5B). The similar redox pair is achieved in the CV of Co_3O_4/Co_9S_8 electrocatalyst. Anodic peak potential at 1.44 V and cathodic at 1.29 V are observed for Co_3O_4/Co_9S_8 catalyst. This pre-oxidative polarization feature of all electrocatalysts may be attributed to oxidation of Co(III) to Co(VI) which indicates an active electrocatalyst structure for OER [57–60]. LSV of Co_3O_4/Co_9S_8 also shows an oxidation peak of this catalyst at 1.44 V (vs. RHE). Further, the values of i_{pa}/i_{pc} and $E_{pa} - E_{pc}$ are calculated from CVs of Co_3O_4, Co_9S_8, and Co_3O_4/Co_9S_8 electrocatalysts. The values of i_{pa}/i_{pc} are >1 for all the electrocatalysts, which indicate that the reactions may be quasi-reversible and not exactly reversible. Furthermore, the values of $E_{pa} - E_{pc}$ are found to be quite greater than 0.059 V, which also confirms that the reactions are quasi-reversible and not precisely reversible. In both LSVs and CVs of all three electrocatalysts, potential values are close to 90 mV calculated at peak width at half of the maximum height ($w_{1/2}$) from oxidation peak, which indicate that peroxidation process of water involves one electron transfer.

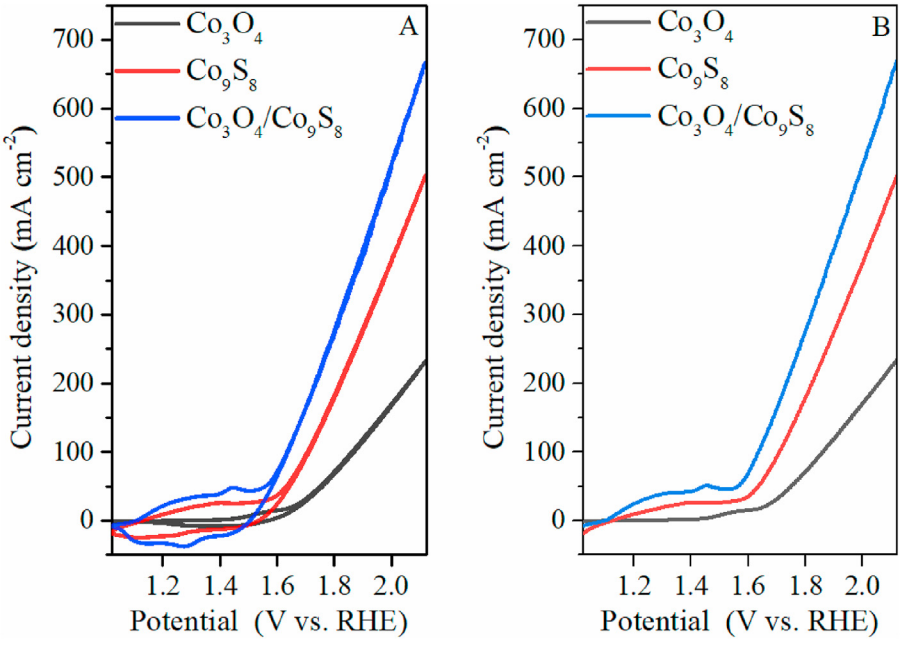

Fig. 5 – The *iR* uncompensated (A) CVs and (B) LSVs observed in 1.0 M solution of KOH for Co_3O_4, Co_9S_8, and Co_3O_4/Co_9S_8 electrocatalysts loaded on Ni-foam.

CV shows the onset potential of OER for Co_3O_4/Co_9S_8 catalyst at 1.50 V vs. RHE. After the onset potential of Co_3O_4/Co_9S_8, the current density grows rapidly and reaches >250 mA cm^{-2} at 1.8 V vs. RHE. Further, increase in the potential sweep to 2 V vs. RHE, the current density increases very sharply and approaches to >500 mA cm^{-2} onto Co_3O_4/Co_9S_8 based electrode. The reason of this enhanced performance could be due to the formation of active Co(IV) centers developed in situ from the oxidation of Co(III), which makes Co_3O_4/Co_9S_8 activation before OER [61]. It is presumed that creation of Co(IV) centers not only shifts the overpotentials (η) of OER toward lower potential but also accelerates the electrochemical water oxidation [57]. Similar active centers of metal ions in higher oxidation state have already been proposed for different OER catalysts based on metals like Fe, Ni and Ir [62–64]. Additionally, preconditioning is not required to gain higher oxidation state of Co, which is required to many others Co-based electrocatalysts already reported. For Co_3O_4 and Co_9S_8 electrocatalysts, the CVs produce catalytic water oxidation current at relatively higher potentials of 1.62 and 1.55 V vs. RHE, respectively. The increase in current density is also not very sharp in case of Co_3O_4 and Co_9S_8 as compared to Co_3O_4/Co_9S_8 electrocatalyst in the higher potential region. A current density of 150 mA cm^{-2} and 300 mA cm^{-2} is obtained at > 2.0 V vs. RHE for Co_3O_4 and Co_9S_8, respectively. Further an oxidation peak is seen in 10 mA cm^{-2} current density region, which obstructs the estimation of η for Co_9S_8 and Co_3O_4/Co_9S_8 electrocatalysts, so η for these catalysts is not reported at this current density. Therefore, a 50 mA cm^{-2} current density is selected to report η for all three catalysts. The values of η for Co_3O_4, Co_9S_8, and Co_3O_4/Co_9S_8 electrocatalysts estimated at 50 mA cm^{-2} current density are 490, 400, and 330 mV, respectively.

It is important to state that the solution resistance is always present in the voltammograms of *i*R uncompensated LSV and CV, so majority of the scientists perform corrections while reporting their results. However, in our opinion, reporting overpotentials values form both *i*R uncompensated and compensated voltammograms for comparison purpose is always better choice. So, the values of solution resistance have been measured by employing EIS and these EIS results are recorded as Nyquist plots in 1 M KOH electrolyte solution at open circuit potential. The results are shown in Fig. 6. Using these plots, the solution resistance values are determined to be 5.0, 3.0, and 2.0 ohm for Co_3O_4, Co_9S_8, and Co_3O_4/Co_9S_8 electrocatalysts, respectively. The *i*R corrected LSVs and CVs of Co_3O_4, Co_9S_8, and Co_3O_4/Co_9S_8 electrocatalysts are obtained by multiplying current with solution resistance values.

The 100% *i*R corrected CVs and LSVs of Co_3O_4, Co_9S_8, and Co_3O_4/Co_9S_8 electrocatalysts loaded on Ni-foam are shown in Fig. 7. From the Fig. 7, an interesting finding is observed, the onset potential values of Co_3O_4, Co_9S_8, and Co_3O_4/Co_9S_8 electrocatalysts are low compared to the values determined from *i*R uncorrected LSVs and CVs. The onset potential values from *i*R compensated CVs are estimated to be 1.58 for Co_3O_4, 1.48 for Co_9S_8, and 1.46 V (vs. RHE) for Co_3O_4/Co_9S_8 electrocatalysts. As per our knowledge, the O_2 evolution onset potential for Co_3O_4/Co_9S_8 (1.46 V vs. RHE) is the lowest reported for most of the cobalt oxide-based water oxidation electrocatalysts [61,65,66]. As the sweeping potential crossed the onset potential, an increase in current density is noticed for all the three electrocatalysts and this rise in current density is much sharper when compared to the current density increase for *i*R uncorrected LSVs and CVs of Co_3O_4, Co_9S_8, and Co_3O_4/Co_9S_8 electrocatalysts. A current density of >100 mA cm^{-2} is attained for Co_3O_4/Co_9S_8 electrocatalyst just at 1.6 V (vs. RHE) and further increase in the potential to 1.8 V vs. RHE, current density rises very sharply, thus approaches to >600 mA cm^{-2}. A current density of >50 mA cm^{-2} and >300 mA cm^{-2} is obtained at > 1.8 V vs. RHE for Co_3O_4 and Co_9S_8, respectively. The values of η for Co_3O_4, Co_9S_8 and Co_3O_4/Co_9S_8 electrocatalysts estimated at 50 mA cm^{-2} current density are 470, 360 and 281 mV, respectively.

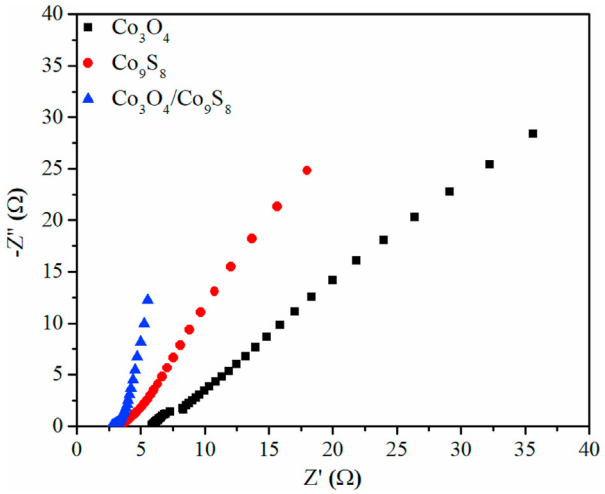

Fig. 6 – EIS Nyquist plots recorded in 1.0 M of KOH solution for Co_3O_4, Co_9S_8, and Co_3O_4/Co_9S_8 electrocatalysts loaded on Ni-foam.

The results obtained from both *i*R uncompensated and compensated CVs and LSVs clearly indicate that Ni-foam modified Co_3O_4/Co_9S_8 electrode efficiently performs electrocatalytic activity for OER. The enhanced performance of Co_3O_4/Co_9S_8 electrocatalyst for OER is associated with several reasons. It may be because of the large surface area of Co_3O_4/Co_9S_8 heterostructure, which induces strong interactions between Co_3O_4 and Co_9O_8 in Co_3O_4/Co_9O_8 heterostructure owing to availability of huge number of sites. Another reason is generation of Co(VI) active center in peroxidation step of water serves as promoter of OER. Further possible reason could be the presence of cavities within its structure, which may function as a pool for electrolyte. Additionally, Co_3O_4/Co_9S_8 heterostructure has lower charge transfer resistance (determined from EIS plots) compared to its counterparts results in enhanced electrocatalytic activity for OER [64].

To understand and learn further insight into the kinetics mechanism of water oxidation, the values of Tafel slopes have been estimated by plotting η vs. Log *j* (Tafel plots) and through slope analysis for Co_3O_4, Co_9O_8 and Co_3O_4/Co_9O_8 electrocatalysts. The Tafel plots are represented in Fig. 8 and the Tafel slope has been estimated to be 37 mV dec^{-1} for Co_3O_4/Co_9O_8 electrocatalyst whereas the Co_3O_4 and Co_9O_8 electrocatalysts exhibit higher Tafel slope values estimated as 95 and 63 mV dec^{-1}, respectively. The smallest Tafel slope (37 mV

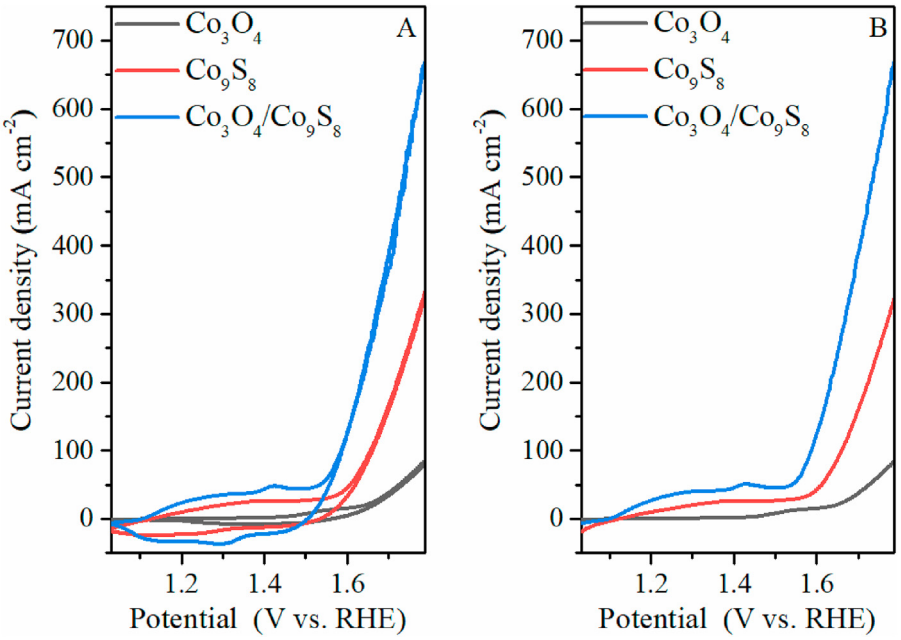

Fig. 7 – The *i*R compensated (A) CVs and (B) LSVs observed in 1.0 M solution of KOH for Co_3O_4, Co_9S_8, and Co_3O_4/Co_9S_8 electrocatalysts loaded on Ni-foam.

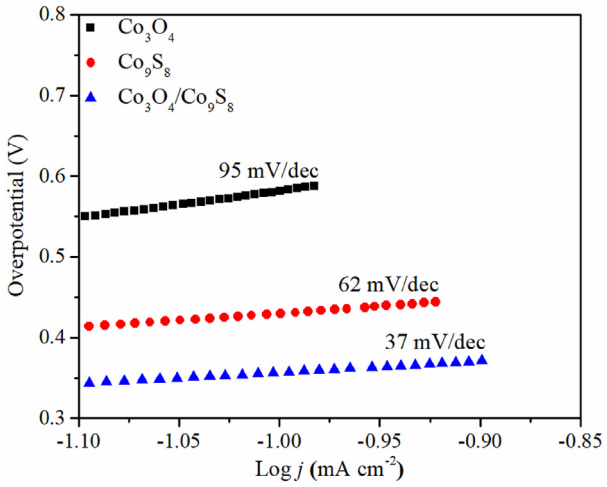

Fig. 8 – Tafel plots for Co_3O_4, Co_9S_8, and Co_3O_4/Co_9S_8 electrocatalysts loaded on Ni-foam.

dec^{-1}) of Co_3O_4/Co_9S_8 electrocatalyst confirms the fast kinetics of electrode process to drive the electrons towards external circuit and indicates that water oxidation is highly efficient and facile for Co_3O_4/Co_9S_8 electrocatalyst under similar set of experimental conditions provided to Co_3O_4 and Co_9O_8 electrocatalysts. Tong et al. reported synthesis of Co_3O_4@Co_9O_8 electrocatalyst using Co_3O_4 nanowires as precursor. The value of over potential for Co_3O_4@Co_9O_8 electrocatalyst estimated at 10 mA cm^{-2} current density was 80 mV with a Tafel slope value of 107.2 mV dec^{-1}during OER process. However, the catalyst Co_3O_4/Co_9S_8 reported in current study shows much better performance towards OER compared to study of Tong et al. [39]. The value of η (281 mV) is estimated at a current density of 50 mA cm^{-2} in alkaline solution with much less value of Tafel slope (37 mV dec^{-1}).

In addition to outstanding catalytic activity of electrocatalyst, an excellent stability of electrocatalyst is another crucial factor and equally important for the performance evaluation of catalysts in view of their commercial applications. To evaluate the stability of Co_3O_4, Co_9S_8, and Co_3O_4/Co_9S_8 electrocatalysts, Chronoamperometry, (i-t) was employed and the results of Chronoamperometry (controlled potential electrolysis) of water oxidation for Co_3O_4, Co_9S_8, and Co_3O_4/Co_9S_8 electrocatalysts are presented in Fig. 9a. For this purpose, a fixed potential value of 1.65 V (vs. RHE) was applied and sustained during the electrolysis of water and measurement of current density. The electrolysis of water was performed for >12 h using Co_3O_4, Co_9S_8, and Co_3O_4/Co_9S_8 electrocatalysts. The stable current densities of 25, 80 and 175 mA cm^{-2} are observed for Co_3O_4, Co_9S_8, and Co_3O_4/Co_9S_8 electrocatalysts, respectively, for a period of >12 h. In current density, no decrease has been detected for all the three electrocatalysts during the given time-period of electrolysis of water. Generally, all the electrocatalysts exhibit excellent stability for prolonged water oxidation however Co_3O_4/Co_9S_8 electrocatalyst is far superior in respect of high current density, low overpotential, small Tafel slope value and low onset potential. Additionally, the Chronoamperometry experiment was performed for Co_3O_4/Co_9S_8 electrocatalyst where a fixed potential value of 1.65 V (vs. RHE) was utilized and electrolysis of water was performed for 50 h (Fig. 9b). A stable current density is observed, and no decrease has been detected during the given time-period of electrolysis of water, which further prove that Co_3O_4/Co_9S_8 electrocatalyst exhibits excellent stability for prolonged water oxidation.

Comparison of OER activities of synthesized catalysts with already published benchmark Cu-based OER catalysts, is

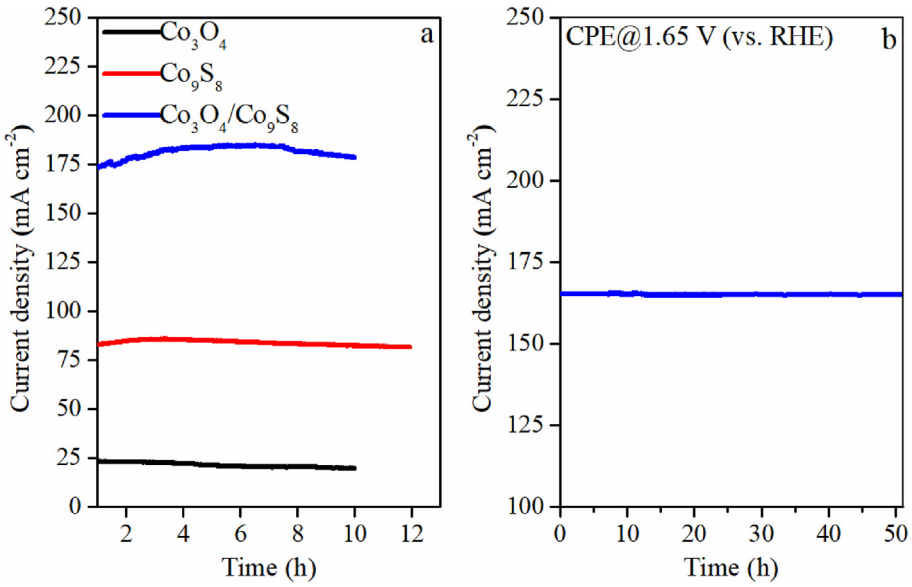

Fig. 9 – (a) Extended period of oxygen evolution during controlled potential electrolysis (1.65 V vs. RHE) at surface of Co_3O_4, Co_9S_8 and Co_3O_4/Co_9S_8 electrocatalysts loaded on Ni-foam in 1.0 M KOH for 12 h and (b) oxygen evolution during controlled potential electrolysis (1.65 V vs. RHE) at Co_3O_4/Co_9S_8 electrocatalysts loaded on Ni-foam in 1.0 M KOH for 50 h.

Table 1 – Comparison of OER activities of Co_3O_4/Co_9S_8 electrocatalyst with already reported Co-based electrocatalysts.

Electrocatalyst	Electrolyte	Onset potential E/V (vs. RHE)	Overpotential η (mV)	Tafel slope b (mV dec^{-1})	Reference
Co_3O_4/Co_9S_8/NF	1.0 M KOH	1.46	281@50 mA cm^{-2}	37	This work
$CoFe_2O_4$/CFP	1.0 M NaOH	–	378@10 mA cm^{-2}	73	[68]
C, N- $CoPO_4$/GC	1.0 M KOH	–	291@10 mA cm^{-2}	57	[69]
CoFeP/GC	1.0 M KOH	1.45	305@10 mA cm^{-2}	49.6	[70]
Cu–$Co(OH)_2$/GC	1.0 M KOH	1.47	300@10 mA cm^{-2}	47	[65]
Co-Fe oxide/GC	1.0 M KOH	~1.55	378@10 mA cm^{-2}	54	[61]
$Co(OH)_2$/CNC	1.0 M KOH	~1.50	300@10 mA cm^{-2}	70.1	[66]
CoO_x/GC	1.0 M KOH + Fe^{3+}	~1.51	309@10 mA cm^{-2}	27.6	[67]

NF= Nickel foam, CFP = Carbon fiber paper, GC = Glassy carbon, CNC = Cu-Ni cloth.

given in Table 1. As highlighted in the table, Co_3O_4/Co_9S_8 heterostructure catalysts exhibits the lowest values of OER performance parameters (onset potential = 1.46 V, overpotential 281 mV@50 mA cm^{-2}, and Tafel slope = 37 mV dec^{-1}) than the other benchmark Co-based catalysts for OER. Although CoO_x/GC catalyst possesses Tafel slope value of only 27.6 mV dec^{-1}, however its overpotential and onset potential is higher than our (Co_3O_4/Co_9S_8) catalyst [67].

Conclusions

In summary, a heterostructure Co_3O_4/Co_9S_8 has been synthesized, evaluated as OER electrocatalyst and compared with its counterparts Co_3O_4 and Co_9S_8 for water oxidation activity. The heterostructure Co_3O_4/Co_9S_8 has been revealed to exhibit outstanding OER with 50 mA cm^{-2} current density at an overpotential of 281 mV, which is exceptionally lower overpotential than that required not only for its counterparts Co_3O_4 (470 mV) and Co_9S_8 (360 mV) but also for many reported Co-based electrocatalysts. Further Co_3O_4/Co_9S_8 has much less Tafel slope (37 mV dec^{-1}) compared to many Co-based electrocatalysts reported in literature. The OER performance of Co_3O_4/Co_9S_8 is credited to several reasons. It may be owing to a large surface area of Co_3O_4/Co_9S_8 heterostructure, that forms strong interaction between Co_3O_4 and Co_9O_8 in Co_3O_4/Co_9O_8 heterostructure due to availability of huge number of sites. Another reason is generation of Co(VI) active center in peroxidation step of water serves as promoter of OER. Further possible reason could be the presence of cavities within its structure, which may function as a pool for electrolyte. Additionally, Co_3O_4/Co_9S_8 heterostructure has lower charge transfer resistance (determined from EIS plots) compared to its counterparts results in enhanced electrocatalytic activity for OER. These findings indicate that heterostructure Co_3O_4/Co_9S_8 has noteworthy advantages in terms of lower over potential, lower Tafel slope, high current density, and stability. These advantages show that heterostructure Co_3O_4/Co_9S_8 is effective enough to compete with the state of art Co-based water oxidation catalysts and there is huge scope for Co-based heterostructures for water oxidation.

Declaration of competing interest

The authors declare that they have no known and unknown competing financial interests that could influence the work reported in this paper.

Acknowledgements

Acknowledgments: The author (A. Dahshan) extends his appreciation to the Deanship of Scientific Research at King Khalid University, Abha, Saudi Arabia for funding this work through research groups program under grant number (RGP.2/179/42).

REFERENCES

[1] Grätzel M. Photoelectrochemical cells. Nature 2001;414:338.
[2] Zhao D, Chen C, Wang C, Junda MM, Song Z, Grice CR, et al. Efficient two-terminal all-perovskite tandem solar cells enabled by high-quality low-bandgap absorber layers. Nature Energy 2018;3:1093–100.
[3] Segev G, Beeman JW, Greenblatt JB, Sharp ID. Hybrid photoelectrochemical and photovoltaic cells for simultaneous production of chemical fuels and electrical power. Nat Mater 2018;17:1115–21.
[4] Gohar RS, Ahmad I, Shah A, Majeed S, Najam-Ul-Haq M, Ashiq MN. Fabrication of transition-metal oxide and chalcogenide nanostructures with enhanced electrochemical performances. J Energy Storage 2020;31:101621.
[5] Ahmad I, Murtaza S, Ahmed S. Electrochemical and photovoltaic study of sunset yellow and tartrazine dyes. Monatsh Chem 2015;146:1631–40.
[6] Ahmad I, Ahmed J, Batool S, Zafar MN, Hanif A, Zahidullah, et al. Design and fabrication of Fe_2O_3/FeP heterostructure for oxygen evolution reaction electrocatalysis. J Alloys Compd 2021:162409.
[7] Huang H, Yu C, Zhao C, Han X, Yang J, Liu Z, et al. Iron-tuned super nickel phosphide microstructures with high activity for electrochemical overall water splitting. Nanomater Energy 2017;34:472–80.
[8] Swierk JR, Mallouk TE. Design and development of photoanodes for water-splitting dye-sensitized photoelectrochemical cells. Chem Soc Rev 2013;42:2357–87.
[9] Suntivich J, May KJ, Gasteiger HA, Goodenough JB, Shao-Horn Y. A perovskite oxide optimized for oxygen evolution catalysis from molecular orbital principles. Science 2011;334:1383–5.
[10] Subbaraman R, Tripkovic D, Chang K-C, Strmcnik D, Paulikas AP, Hirunsit P, et al. Trends in activity for the water electrolyser reactions on 3d M (Ni, Co, Fe, Mn) hydr (oxy) oxide catalysts. Nat Mater 2012;11:550.
[11] Li Y, Hu L, Zheng W, Peng X, Liu M, Chu PK, et al. Ni/Co-based nanosheet arrays for efficient oxygen evolution reaction. Nanomater Energy 2018;52:360–8.
[12] Xiong X, You C, Liu Z, Asiri AM, Sun X. Co-doped CuO nanoarray: an efficient oxygen evolution reaction electrocatalyst with enhanced activity. ACS Sustainable Chem Eng 2018;6:2883–7.
[13] Cui B, Lin H, Li JB, Li X, Yang J, Tao J. Core–ring structured $NiCo_2O_4$ nanoplatelets: synthesis, characterization, and electrocatalytic applications. Adv Funct Mater 2008;18:1440–7.
[14] Liang J, Liu Q, Li T, Luo Y, Lu S, Shi X, et al. Magnetron sputtering enabled sustainable synthesis of nanomaterials for energy electrocatalysis. Green Chem 2021;23:2834–67.
[15] Li X, Zhao H, Liang J, Luo Y, Chen G, Shi X, et al. A-site perovskite oxides: an emerging functional material for electrocatalysis and photocatalysis. J Mater Chem 2021;9:6650–70.
[16] Stoerzinger KA, Rao RR, Wang XR, Hong WT, Rouleau CM, Shao-Horn Y. The role of Ru redox in pH-dependent oxygen evolution on rutile ruthenium dioxide surfaces. Inside Chem 2017;2:668–75.
[17] Park H-S, Yang J, Cho MK, Lee Y, Cho S, Yim S-D, et al. RuO_2 nanocluster as a 4-in-1 electrocatalyst for hydrogen and oxygen electrochemistry. Nanomater Energy 2019;55:49–58.
[18] Liu K, Zhang C, Sun Y, Zhang G, Shen X, Zou F, et al. High-performance transition metal phosphide alloy catalyst for oxygen evolution reaction. ACS Nano 2018;12:158–67.
[19] Morales-Guio CG, Liardet L, Hu X. Oxidatively electrodeposited thin-film transition metal (oxy) hydroxides as oxygen evolution catalysts. J Am Chem Soc 2016;138:8946–57.
[20] Joya KS, Takanabe K, De Groot HJ. Surface generation of a cobalt-derived water oxidation electrocatalyst developed in a neutral HCO_3^-/CO_2 system. Adv Energy Mater 2014;4:1400252.
[21] Xue Y, Huang B, Yi Y, Guo Y, Zuo Z, Li Y, et al. Anchoring zero valence single atoms of nickel and iron on graphdiyne for hydrogen evolution. Nat Commun 2018;9:1460.
[22] Hui L, Xue Y, Yu H, Liu Y, Fang Y, Xing C, et al. Highly efficient and selective generation of ammonia and hydrogen on a graphdiyne-based catalyst. J Am Chem Soc 2019;141:10677–83.
[23] Fang Y, Xue Y, Hui L, Yu H, Li Y. Graphdiyne@Janus magnetite for photocatalytic nitrogen fixation. Angew Chem Int Ed 2021;60:3170–4.
[24] Ye C, Zhang L, Yue L, Deng B, Cao Y, Liu Q, et al. A NiCo LDH nanosheet array on graphite felt: an efficient 3D electrocatalyst for the oxygen evolution reaction in alkaline media. Inorg Chem Front 2021;8:3162–6.
[25] Xie J, Xie Y. Transition metal nitrides for electrocatalytic energy conversion: opportunities and challenges. Chem Eur J 2016;22:3588–98.
[26] Zhao Y, Jia X, Chen G, Shang L, Waterhouse GI, Wu L-Z, et al. Ultrafine NiO nanosheets stabilized by TiO_2 from monolayer NiTi-LDH precursors: an active water oxidation electrocatalyst. J Am Chem Soc 2016;138:6517–24.
[27] Görlin M, Chernev P, Ferreira de Araújo J, Reier T, Dresp Sr, Paul B, et al. Oxygen evolution reaction dynamics, faradaic charge efficiency, and the active metal redox states of Ni–Fe oxide water splitting electrocatalysts. J Am Chem Soc 2016;138:5603–14.
[28] Meng C, Cao Y, Luo Y, Zhang F, Kong Q, Alshehri AA, et al. A Ni-MOF nanosheet array for efficient oxygen evolution electrocatalysis in alkaline media. Inorg Chem Front 2021;8:3007–11.
[29] Cao Y, Wang T, Li X, Zhang L, Luo Y, Zhang F, et al. A hierarchical CuO@NiCo layered double hydroxide core–shell nanoarray as an efficient electrocatalyst for the oxygen evolution reaction. Inorg Chem Front 2021;8:3049–54.
[30] Wang J, Ma X, Qu F, Asiri AM, Sun X. Fe-doped Ni_2P nanosheet array for high-efficiency electrochemical water oxidation. Inorg Chem 2017;56:1041–4.
[31] Wei Y, Ren X, Ma H, Sun X, Zhang Y, Kuang X, et al. $CoC_2O_4.2H_2O$ derived Co_3O_4 nanorods array: a high-efficiency 1D electrocatalyst for alkaline oxygen evolution reaction. Chem Commun 2018;54:1533–6.
[32] Feng Y, He T, Alonso-Vante N. In situ free-surfactant synthesis and ORR-electrochemistry of carbon-supported Co_3S_4 and $CoSe_2$ nanoparticles. Chem Mater 2007;20:26–8.

[33] Liang L, Cheng H, Lei F, Han J, Gao S, Wang C, et al. Metallic single-unit-cell orthorhombic cobalt diselenide atomic layers: robust water-electrolysis catalysts. Angew Chem Int Ed 2015;54:12004–8.
[34] Tong Y, Chen P, Zhou T, Xu K, Chu W, Wu C, et al. A bifunctional hybrid electrocatalyst for oxygen reduction and evolution: cobalt oxide nanoparticles strongly coupled to B, N-decorated graphene. Angew Chem 2017;129:7227–31.
[35] Zhang X, Liu R, Zang Y, Liu G, Wang G, Zhang Y, et al. Co/CoO nanoparticles immobilized on Co–N-doped carbon as trifunctional electrocatalysts for oxygen reduction, oxygen evolution and hydrogen evolution reactions. Chem Commun 2016;52:5946–9.
[36] Liu Y, Xiao C, Lyu M, Lin Y, Cai W, Huang P, et al. Ultrathin Co_3S_4 nanosheets that synergistically engineer spin states and exposed polyhedra that promote water oxidation under neutral conditions. Angew Chem Int Ed 2015;54:11231–5.
[37] Pu J, Shen Z, Zheng J, Wu W, Zhu C, Zhou Q, et al. Multifunctional Co_3S_4@sulfur nanotubes for enhanced lithium-sulfur battery performance. Nanomater Energy 2017;37:7–14.
[38] Sivanantham A, Ganesan P, Shanmugam S. Hierarchical $NiCo_2S_4$ nanowire arrays supported on Ni foam: an efficient and durable bifunctional electrocatalyst for oxygen and hydrogen evolution reactions. Adv Funct Mater 2016;26:4661–72.
[39] Tong Y-L, Xing L, Dai M-Z, Wu X. Hybrid Co_3O_4@Co_9S_8 electrocatalysts for oxygen evolution reaction. Front Mater 2019;6:233.
[40] Deng S, Shen S, Zhong Y, Zhang K, Wu J, Wang X, et al. Assembling Co_9S_8 nanoflakes on Co_3O_4 nanowires as advanced core/shell electrocatalysts for oxygen evolution reaction. J Energy Chem 2017;26:1203–9.
[41] Ahmad I, Shah SM, Ashiq MN, Khan RA. Effect of Nd^{3+} and Cd^{2+} ions co-substitution on the dielectric and electron transport properties of spinel strontium nanoferrites. Ceram Int 2016;42:12763–70.
[42] Ahmad I, Shah SM, Zafar MN, Ullah S, Ul-Hamid A, Ashiq MN, et al. Fabrication of highly resistive La–Zn co-substituted spinel strontium nanoferrites for high frequency devices applications. Mater Chem Phys 2021;259:124031.
[43] Ahmad I, Shah SM, Zafar MN, Ashiq MN, Tang W, Jabeen U. Synthesis, characterization and charge transport properties of Pr–Ni Co-doped $SrFe_2O_4$ spinel for high frequency devices applications. Ceram Int 2021;47:3760–71.
[44] Ahmad I, Shah SM, Ashiq MN, Nawaz F, Shah A, Siddiq M, et al. Fabrication of Nd^{3+} and Mn^{2+} ions Co-doped spinal strontium nanoferrites for high frequency device applications. J Electron Mater 2016;45:4979–88.
[45] Ahmed S, Ahmad I, Ahmad Z, Jalil A, Ashiq MN, Shafique A. Fabrication and corrosion inhibition behavior of hierarchical Al-Cr co-doped magnesium ferrites nanomaterial for steel. Surf Coating Technol 2021;405:126687.
[46] Aloqayli S, Ranaweera C, Wang Z, Siam K, Kahol P, Tripathi P, et al. Nanostructured cobalt oxide and cobalt sulfide for flexible, high performance and durable supercapacitors. Energy Storage Mater 2017;8:68–76.
[47] Pudukudy M, Yaakob Z. Sol-gel synthesis, characterisation, and photocatalytic activity of porous spinel Co_3O_4 nanosheets. Chem Paper 2014;68:1087–96.
[48] Dileep NP, Vineesh TV, Sarma PV, Chalil MV, Prasad CS, Shaijumon MM. Electrochemically exfoliated β-$Co(OH)_2$ nanostructures for enhanced oxygen evolution electrocatalysis. ACS Appl Energy Mater 2020;3:1461–7.
[49] Tannenbaum R, Zubris M, David K, Ciprari D, Jacob K, Jasiuk I, et al. FTIR characterization of the reactive interface of cobalt oxide nanoparticles embedded in polymeric matrices. J Phys Chem B 2006;110:2227–32.
[50] Khan SB, Faisal M, Rahman MM, Jamal A. Low-temperature growth of ZnO nanoparticles: photocatalyst and acetone sensor. Talanta 2011;85:943–9.
[51] Chen X, Shen Y, Zhang W, Zhang J, Wei D, Lu R, et al. In-situ growth of ZnO nanowire arrays on the sensing electrode via a facile hydrothermal route for high-performance NO_2 sensor. Appl Surf Sci 2018;435:1096–104.
[52] Linganiso EC, Mwakikunga BW, Coville NJ, Mhlanga SD. Observation of the structural, optical and magnetic properties during the transformation from hexagonal NiS nano-compounds to cubic NiO nanostructures due to thermal oxidation. J Alloys Compd 2015;629:131–9.
[53] Tang Y, Chen T, Yu S, Qiao Y, Mu S, Zhang S, et al. A highly electronic conductive cobalt nickel sulphide dendrite/quasi-spherical nanocomposite for a supercapacitor electrode with ultrahigh areal specific capacitance. J Power Sources 2015;295:314–22.
[54] Wang G, Cao D, Yin C, Gao Y, Yin J, Cheng L. Nickel foam supported-Co_3O_4 nanowire arrays for H_2O_2 electroreduction. Chem Mater 2009;21:5112–8.
[55] Sharma S, Garg N, Ramanujachary KV, Lofland SE, Ganguli AK. Design of anisotropic Co_3O_4 nanostructures: control of particle size, assembly, and aspect ratio. Cryst Growth Des 2012;12:4202–10.
[56] Dong C, Yi Q, Shen B, Xing M, Zhang J. Novel Fenton process of Co-catalyst Co_9S_8 quantum dots for highly efficient removal of organic pollutants. Chemosphere 2020:128648.
[57] Yeo BS, Bell AT. Enhanced activity of gold-supported cobalt oxide for the electrochemical evolution of oxygen. J Am Chem Soc 2011;133:5587–93.
[58] Chivot J, Mendoza L, Mansour C, Pauporté T, Cassir M. New insight in the behaviour of Co–H_2O system at 25–150 °C, based on revised Pourbaix diagrams. Corrosion Sci 2008;50:62–9.
[59] Foelske A, Strehblow H-H. Structure and composition of electrochemically prepared oxide layers on Co in alkaline solutions studied by XPS. Surf Interface Anal 2002;34:125–9.
[60] Bewick A, Gutiérrez C, Larramona G. An in-situ IR spectroscopic study of the anodic oxide film on cobalt in alkaline solutions. J Electroanal Chem 1992;333:165–75.
[61] Budiyanto E, Yu M, Chen M, DeBeer S, Rüdiger O, Tüysüz H. Tailoring morphology and electronic structure of cobalt iron oxide nanowires for electrochemical oxygen evolution reaction. ACS Appl Energy Mater 2020;3:8583–94.
[62] Nakagawa T, Beasley CA, Murray RW. Efficient electro-oxidation of water near its reversible potential by a mesoporous IrOx nanoparticle film. J Phys Chem C 2009;113:12958–61.
[63] Lyons MEG, Brandon MP. A comparative study of the oxygen evolution reaction on oxidised nickel, cobalt and iron electrodes in base. J Electroanal Chem 2010;641:119–30.
[64] Khan NA, Rashid N, Junaid M, Zafar MN, Faheem M, Ahmad I. NiO/NiS heterostructures: an efficient and stable electrocatalyst for oxygen evolution reaction. ACS Appl Energy Mater 2019;2:3587–94.
[65] Chen L, Zhang H, Chen L, Wei X, Shi J, He M. Facile synthesis of Cu doped cobalt hydroxide (Cu–$Co(OH)_2$) nano-sheets for efficient electrocatalytic oxygen evolution. J Mater Chem 2017;5:22568–75.
[66] Wang Z, Ji S, Liu F, Wang H, Wang X, Wang Q, et al. Highly efficient and stable catalyst based on $Co(OH)_2$@Ni

electroplated on Cu-metallized cotton textile for water splitting. ACS Appl Mater Interfaces 2019;11:29791–8.
[67] Gong L, Chng XYE, Du Y, Xi S, Yeo BS. Enhanced catalysis of the electrochemical oxygen evolution reaction by iron (III) ions adsorbed on amorphous cobalt oxide. ACS Catal 2018;8:807–14.
[68] Kargar A, Yavuz S, Kim TK, Liu C-H, Kuru C, Rustomji CS, et al. Solution-processed $CoFe_2O_4$ nanoparticles on 3D carbon fiber papers for durable oxygen evolution reaction. ACS Appl Mater Interfaces 2015;7:17851–6.
[69] Huang Z-Q, Lu W-X, Wang B, Chen W-J, Xie J-L, Pan D-S, et al. A mesoporous C,N-co doped Co-based phosphate ultrathin nanosheet derived from a phosphonate-based-MOF as an efficient electrocatalyst for water oxidation. Catal Sci Technol 2019;9:4718–24.
[70] Xu H, Wei J, Liu C, Zhang Y, Tian L, Wang C, et al. Phosphorus-doped cobalt-iron oxyhydroxide with ultrafine nanosheet structure enable efficient oxygen evolution electrocatalysis. J Colloid Interface Sci 2018;530:146–53.